VIP Layered Structures Very Important Paper

Deutsche Ausgabe: DOI: 10.1002/ange.201510432
Internationale Ausgabe: DOI: 10.1002/anie.201510432

A Two-Dimensional Zirconium Carbide by Selective Etching of Al_3C_3 from Nanolaminated $Zr_3Al_3C_5$

Jie Zhou[+], Xianhu Zha[+], Fan Y. Chen, Qun Ye, Per Eklund, Shiyu Du, and Qing Huang**

Abstract: *The room-temperature synthesis of a new two-dimensional (2D) zirconium-containing carbide, $Zr_3C_2T_z$ MXene is presented. In contrast to traditional preparation of MXene, the layered ternary $Zr_3Al_3C_5$ material instead of MAX phases is used as source under hydrofluoric acid treatment. The structural, mechanical, and electronic properties of the synthesized 2D carbide are investigated, combined with first-principles density functional calculations. A comparative study on the structrual stability of our obtained 2D $Zr_3C_2T_z$ and $Ti_3C_2T_z$ MXenes at elevated temperatures is performed. The obtained 2D $Zr_3C_2T_z$ exhibits relatively better ability to maintain 2D nature and strucural integrity compared to Ti-based Mxene. The difference in structural stability under high temperature condition is explained by a theoretical investigation on binding energy.*

During the past decade, two-dimensional (2D) materials have attracted extensive attention owing to their high surface area to volume ratio, unique electronic structures, and physiochemical properties derived from their low dimensionality.[1–7] Graphene, the most studied 2D material with ultrahigh mechanical strength[8,9] and excellent electronic and thermal conductivities,[1,10,11] exhibits potential applications in electrochemical energy storage, transparent electrodes, and nano-composites.[12] However, owing to its intrinsic zero band gap and simple chemistry, applications of graphene are restricted in some aspects, such as field-effect transistors.[10] Thus, investigations on other 2D materials are performed, especially for those 2D materials with two or more composition elements, such as metal oxides, layered metal chalcogenides (LMDCs), hexagonal boron nitride (BN), and hydroxides.[6,13] In recent years, a new class of 2D materials, called MXenes, have emerged.[14] Members in this family are described by the general formula of $M_{n+1}X_nT_z$ (wherein M is an early transition metal, X is C and/or N, n is 1, 2, 3, and T_z denotes surface terminated functional groups).[14] Generally, MXenes are produced by the selective etching of Al layers from their parental layered ternary MAX phases, a large group which comprises more than 70 members.[15,16] Through selective etching of aluminum layers, experimental investigations have successfully identified about 10 different MXenes: $Ti_3C_2T_z$, Ti_2CT_z, $Ta_4C_3T_z$, $TiNbCT_z$, $(V_{0.5},Cr_{0.5})_3C_2T_z$, Ti_3CNT_z, Nb_2CT_z, V_2CT_z, and $Nb_4C_3T_z$.[14,17] Most of the synthesized MXenes are metallic,[18] hydrophilic, and predicted to have high elastic moduli, implying potential application as reinforcement of polymer.[19,20] The existance of Dirac electrons in some MXenes has also been theoretically predicted.[21] Moreover, similar to graphene, MXenes are promising candidate electrode materials for lithium-ion batteries and supercapacitors by facile intercalation of Li ions into the MXene layers.[22–27] Recently, considerable efforts have been made to further expand the family of 2D carbides. On the basis of a substitutional solid solution method, Gogotsi and Barsoum et al.[28] successfully synthesized $Mo_2TiC_2T_z$, $Mo_2Ti_2C_3T_z$, and $Cr_2TiC_2T_z$ MXenes, and surface dependent electrochemical behaviors in the case of $Mo_2TiC_2T_z$ have been revealed. Moreover, Mo_2CT_z MXene[29] has been synthesized through selective etching of gallium (Ga) from a thin film of the new ternary nanolaminated Mo_2Ga_2C.[30,31] Besides, large-area high-quality 2D α-Mo_2C, WC, and TaC crystals have been fabricated by a chemical vapour deposition (CVD) process.[32] However, potential MXene compounds in materials systems where Al-containing MAX phases are not established, such as Hf_2C and Zr_2C, are yet to be produced.

Herein, for the first time, we report the preparation of Zr-containing 2D carbide based on selective extraction of Al-C units from an alternative layered ternary $Zr_3Al_3C_5$, benefiting from the relatively weakly bonded and hydrolysis-prone Al-C layers in the $Zr_3Al_3C_5$ crystal structure. $Zr_3Al_3C_5$ is a typical member of the layered ternary and quaternary transition-metal carbides beyond MAX phases; holding a common formula of $M_nAl_3C_2$ and $M_n[Al(Si)]_4C_3$ (where M = Zr or Hf, $n = 1$–3).[33] The crystal structure of these carbides can be described as an intergrowth structure of layers with hexagonal MC and Al_4C_3-like $Al_3C_2/[Al(Si)]_4C_3$ sharing a carbon monolayer at their coupling boundaries.[33]

We prepared $Zr_3Al_3C_5$ by an in situ reactive pulsed electric current sintering (PECS) process (Supporting Information, Section S1) similar to our previous study.[34] The exfoliation process of $Zr_3Al_3C_5$ was implemented by using concentrated hydrofloric (HF) acid. The structural, electronic, and elastic properties of the as-exfoliated nanosheets were investigated combined with first-principles density functional calculations. Moreover, the structural stability of the as-prepared nanosheets at elevated temperatures were studied and compared with that of $Ti_3C_2T_z$ MXenes.

[*] J. Zhou,[+] X. H. Zha,[+] F. Y. Chen, Q. Ye, Prof. S. Y. Du, Prof. Q. Huang
Engineering Laboratory of Specialty Fibers and Nuclear Energy Materials (FiNE), Ningbo Institute of Materials Engineering and Technology, Chinese Academy of Sciences
Ningbo, Zhejiang 315201 (China)
E-mail: dushiyu@nimte.ac.cn
huangqing@nimte.ac.cn
Prof. P. Eklund
Thin Film Physics Division, Linköping University, IFM
58183 Linköping (Sweden)

[+] These authors contributed equally to this work.

Supporting information for this article can be found under http://dx.doi.org/10.1002/anie.201510432.

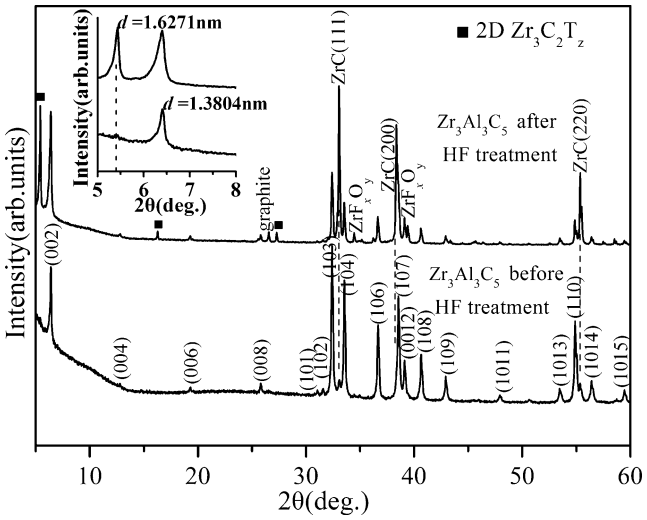

Figure 1. X-ray diffraction patterns of $Zr_3Al_3C_5$ before and after HF treatment.

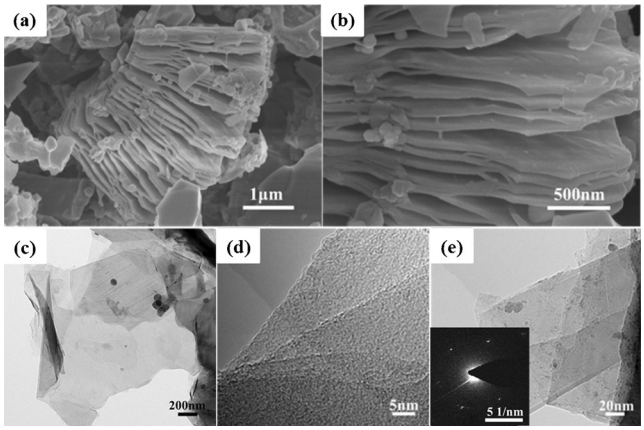

Figure 2. a), b) SEM images of the powders after HF treatment, showing the exfoliated grain and accordion-like structure; c) Typical bright-field TEM images of the 2D $Zr_3C_2T_z$ after ultrasonication; d) TEM image of few-layered $Zr_3C_2T_z$ and e) TEM image of a scrolled $Zr_3C_2T_z$ nanosheet. Inset in (e) is a SAED pattern showing the reserved hexagonal basal plane symmetry.

As shown in Figure 1, the as-fabricated powders are predominantly single-phase $Zr_3Al_3C_5$ besides a minor amount of ZrC impurities. When the $Zr_3Al_3C_5$ powders (300 mesh) were immersed in 50 wt% hydrofluric acid (HF) aqueous solution, bubbles, possibly being H_2 and CH_4, were observed, which had also been observed during the formation of Ti_3C_2 MXenes.[19] Details of the etching process can be found in the Supporting Information, Section S1. The corresponding XRD result of the etched powders is plotted in Figure 1. The peak intensities originating from the parent $Zr_3Al_3C_5$ crystal decrease substantially after immersion in the concentrated HF solution. More importantly, the (0002) peak downshifts to a lower angle of $2\theta = 5.43°$, attributing to an enlarged *c* lattice parameter of 32.53 Å, from the original 27.73 Å of $Zr_3Al_3C_5$ crystal. The newly emerged low-angle (0002) peak is typical for most reported HF-etched MXenes,[17,19] another two (000l) peaks located at $2\theta = 16.32°$, and $2\theta = 27.24°$ can also be detected, respectively. Unlike the broad peaks typical of HF-etched MXenes, three new ly formed lower angle (000l) peaks in our present study shows relatively sharper shape and increased intensity, which is more typical of intercalated MXenes.[27,35] It is thus reasonable to speculate that the enlarged *c* lattice parameter of 32.53 Å might be associated with spontaneous intercalation during the etching process.[27] Moreover, the small amount of rock-salt-like cubic ZrC impurities presented in the raw $Zr_3Al_3C_5$ powders did not react with HF and the relative intensity of their peaks increases apparently after HF-treatment, which is probably due to a drastic loss of parent $Zr_3Al_3C_5$ and possibly formation of less ordered phase.

The SEM images of $Zr_3Al_3C_5$ after the HF treatment (Figure 2 a, b) confirm exfoliation of individual grain along the basal planes. Grain with accordion morphology are observed, which is similar to what was reported for Ti_3AlC_2.[19] The corresponding energy dispersive spectrum (EDS) results obtained from an area of about 2000 μm^2 show the presence of Zr, C, O, F, and corresponding substantial decrease of the Al signal (Supporting Information, Figure S4), indicates the removal of Al-C layer from the original crystal structure.[19]

Additionaly, the obtained Zr/Al molar ratio was larger than 3.0:0.9. In consideration of the possible residual aluminum fluoride,[26] it is reasonable to assume that more than 70 at% of the $Zr_3Al_3C_5$ has been transformed.[26] TEM images of HF-etched $Zr_3Al_3C_5$ after sonication are shown in Figure 2 c–e, depicting electron-transparent thin morphology and a few layer structures, EDS results of the same flake confirm the presence of Zr, C, and O with no aluminum (Supporting Information, Figure S5). Moreover, the thin nanosheet is presented to be flexible and folding, which is similar to those of graphene and 2D MXenes.[19,36] The corresponding selected-area electron diffraction (SAED, inset in Figure 2 e) shows the hexagonal symmetry of the as-obtained nanosheets.[33]

The Zr 3d and O 1s X-ray photoelectron spectroscopy (XPS) results before and after HF treatment are shown in Figure 3 a. The presence of Zr−C and Zr−O bonds before treatment matches previous works on ZrC[37] (Figure 3 a,b).

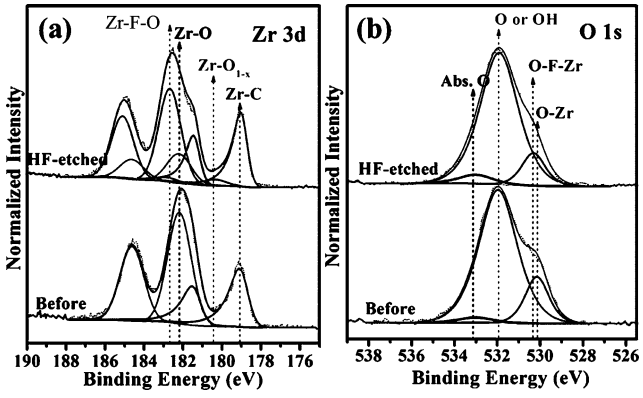

Figure 3. High-resolution XPS spectra of samples before and after etching treatment in the a) Zr 3d region and b) O 1s region.

After HF treatment, the fitted results of XPS spectrum in the Zr 3d region consistently show the appearence of mixed Zr-F-O,[38] partially oxidized Zr-O,[37] and Zr−C bonds[37] (Figure 3a). Furthermore, the corresponding fitted results in the O 1s region further comfirm the presence of mixed Zr-F-O[38] in etched samples, partially oxidized Zr−O bonds and OH groups[37] (Figure 3b) are also presented in both spectra, indicating the potential formation of Zr_3C_2 and a mixture of F and OH surface groups.[26] Moreover, Zr−C bond emerges in the C 1s region accordingly[38] (Supporting Information, Figure S1).

Based on the aformentioned results, it is reasonable to deduce that the relatively weakly bonded and easily hydrolyzed Al-C slabs in $Zr_3Al_3C_5$ were selectively etched when immersed in 50% HF solution, and the surface of left Zr-based layer was functionalized by OH and F surface groups.

It should be noted that there is one 2D carbon atomic plane shared by Zr-C layers and Al_3C_2 slab in the unit cell of $Zr_3Al_3C_5$ as mentioned above. To exactly verify the affiliation of the C atoms during the etching process and thus determine the final reaction product, density functional theory (DFT)-based geometry optimization was carried out. Figure 4a

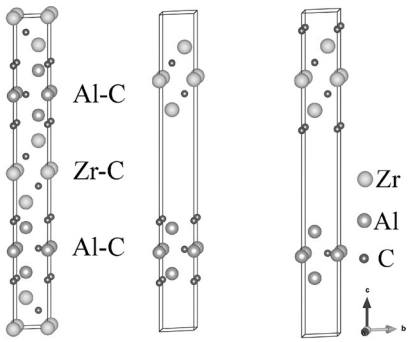

Figure 4. a) The unit cell of $Zr_3Al_3C_5$; b) Model A: $Zr_3C_2 + Al_3C_3$; c) Model B: $Zr_3C_4 + Al_3C$.

shows the crystal structure of parent $Zr_3Al_3C_5$.[33] Two models, named Model A and Model B, are considered and given in Figure 4b and c, respectively. In Model A, the concerned carbon layers combined with aluminum atoms, which means the dissolved layers are Al_3C_3 in hydrofluoric acid and our product is $Zr_3C_2T_z$ MXene. Reversely, Model B shows the other possibility that the carbon layers are retained after hydrofluoric acid treatment. In these two models, a vacuum layer of 10 Å between the separated monolayers is used to eliminate the layer interaction. After optimization, the total energy of Model A is determined to be −80.03 eV, and that of model B is −76.85 eV. Evidently, Model A is more stable than Model B, which implies that our monolayer product is 2D $Zr_3C_2T_z$. On the basis of the above analysis, the structural transformation process of $Zr_3Al_3C_5$ under HF treatment is illustrated in the Supporting Information, Figure S2. Since the thickness of the dissolved Al_3C_3 slab is much thicker than that of monolayer aluminum in the unit cell of MAX phase,[19] more interlayer space are provided. Furthermore, the relatively small lateral size of the obtained sheets also favors the occurance of intercalation process. It should be noted that the large observed *c* lattice parameters (32.53 Å) in our present study can be attributed to spontaneous intercalation of water molecules[17,26,39] and cointercalation of reaction products into the 2D $Zr_3C_2T_z$ during the etching process, which have been reported for the preparation of V_2C,Nb_2C, and Mo_2C MXenes.[26,29]

On the basis of the above experimental and calculated results, the chemical reactions occurred during the etching process of $Zr_3Al_3C_5$ can be reasonably described by the following simplified equations:

$$Zr_3Al_3C_5 + HF \rightarrow AlF_3 + CH_4 + Zr_3C_2 \quad (1)$$

$$Zr_3C_2 + H_2O \rightarrow Zr_3C_2(OH)_2 + H_2 \quad (2)$$

$$Zr_3C_2 + HF \rightarrow Zr_3C_2F_2 + H_2 \quad (3)$$

which is similar to the reactions occurred during the HF etching process of Ti_3AlC_2 powders.[19]

To further explore the exact thickness of the as-etched $Zr_3C_2T_z$, AFM measurement was carried out for the $Zr_3C_2T_z$ samples after sonication (Supporting Information, Figure S3). The thickness of the Zr3C2Tz was approximately 3.5 nm (nearly corresponds to two layers of $Zr_3C_2T_z$), which is approximately the calculated *c* value based on XRD patterns (Figure 1), and the lateral size of the nanosheets was approximately 1.5–2 μm.

The structural stability of 2D materials is important for their practical applications at elevated temperatures. Thus a comparative study on the structural stability of 2D $Ti_3C_2T_z$ and $Zr_3C_2T_z$ MXenes under high temperatures was performed. Figure 5a shows thermal gravimetry (TG) and differential scanning calorimetry (DSC) curves of $Ti_3C_2T_z$ and $Zr_3C_2T_z$ from room temperatue to 1200 °C in argon atmosphere. In the case of $Ti_3C_2T_z$, the first stage of mass loss about 7% can be observed in the 50–200 °C temperature range. Concomitantly, an endothermic peak emerges at 133 °C in the corresponding DSC curve. Regarding 2D $Zr_3C_2T_z$ MXene, one stage of mass loss of about 4% in the 50–500 °C temperature range emerges in TG curve. Furthermore, an endothermic peak appears at 71 °C in its corresponding DSC curve. It is reasonable to conclude that the first stage in both cases is due to the removal of physically absorbed water[26,40,41] and intercalated crystal water.[35] Above 500 °C, a broad exothermic peak at about 700 °C can be identified in DSC curve of 2D $Zr_3C_2T_z$, and without apprent mass loss in TG curve from 500 °C to 1200 °C. This slow exothermic process might be related to the growth of nanocrystals. In the case of $Ti_3C_2T_z$, an apparent mass loss of about 6% occurred in the 200–800 °C temperature range, indicating the potential dehydroxylation of residual-isolated OH groups bonded with the metal-terminated surface.[41] It is followed by an abrupt mass loss of about 14% from 800 to 1000 °C. Simultaneously, a relatively sharp exothermic peak appears at about 984 °C in DSC curves, which is most likely related to crystal structure transformation.[15,40] Note that in the case of $Zr_3C_2T_z$, the relatively less significant mass loss in TG curves could be related to the influence of the more stable pre-existing cubic

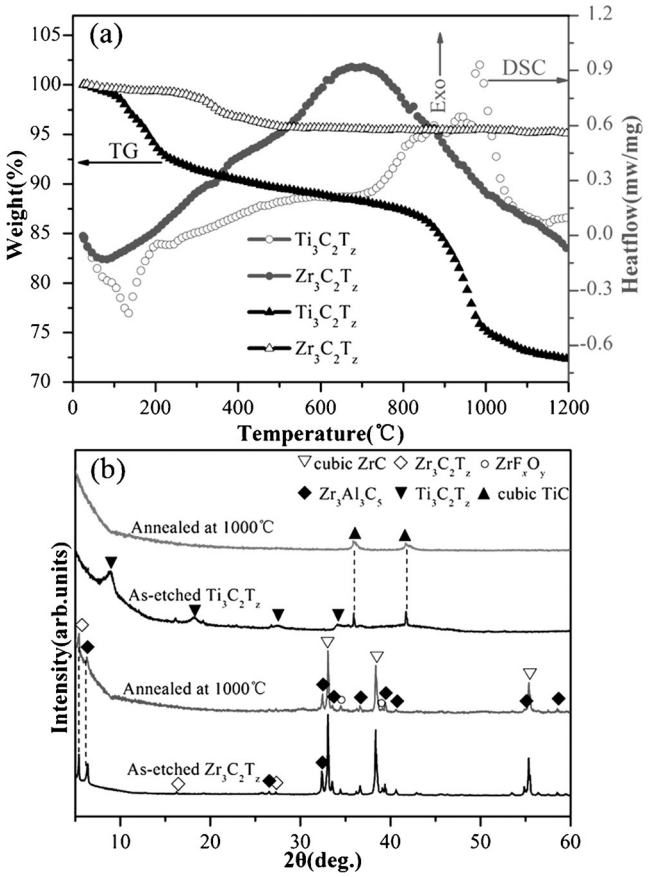

Figure 5. a) TG and DSC curves of Ti_3C_2 and 2D $Zr_3C_2T_z$ from RT to 1200 °C in argon atmosphere, b) X-ray diffraction patterns of Ti_3C_2 MXene and 2D $Zr_3C_2T_z$ before and after annealed in vacuum at 1000 °C for 2 h.

ZrC and residual $Zr_3Al_3C_5$ second phases presented in the HF-treated powder mixture.

To further gain insight in the above distinct thermal behaviors between the $Ti_3C_2T_z$ and $Zr_3C_2T_z$ MXenes in the 500–1000 °C temperature range, XRD analysis was performed. As shown in Figure 5b, it can be seen that characteristic diffraction peaks belong to hexagonally symmetrical Ti_3C_2 MXenes disappeared and only cubic TiC can be detected after two hours of vacuum annealing at 1000 °C. This indicates apparent decrease of order of Ti_3C_2 MXenes along c axis or that a structural transformation occurred. In the case of $Zr_3C_2T_z$ (Figure 5b), peaks corresponding to $Zr_3C_2T_z$ still can be detected, but with decreases intensity and broadened, indicating removal of intercalated species, surface groups, and less order along *c*-axis. Moreover, diffraction peaks related to residual $Zr_3Al_3C_5$ are also decreased to some extent, which could be related to initial structural damage occurred during the HF etching process and subsequent high temperature pertubation.

To exactly identify the above structural evolution, we performed TEM observation of the samples after vacuum annealing treatment. A TEM image of ultrasonicated $Ti_3C_2T_z$ nanosheets (Figure 6a) shows that their 2D nature and structural integrity to be partially disturbed. The corresponding SAED (inset in Figure 6a) can be indexed as cubic TiC_x, indicating that a structural transformation has occured. In fact, similar hexagonal-cubic structural transformation was observed in previous studies, in those cases, bulk Ti_3SiC_2 was immersed in molten aluminum[42] or cryolite[43] at high temperatures. Figure 6b shows that some nanocrystals formed on the initial $Ti_3C_2T_z$ flakes, SAED analysis (inset in Figure 6b) reveals the formation of rutile TiO_2, which might be related to the oxidation of nanosheet from oxidizing surface groups or residual oxygen in vacuum. As shown in Figure 6c, nanosheets of $Zr_3C_2T_z$ after HT treatment remain their quite thin and uniform morphology, which is similar to that of the untreated state. The corresponding SAED (inset in Figure 6c) confirms the original hexagonal symmetry. It is thus reasonable that $Zr_3C_2T_z$ exhibits better structural integrity, and remains 2D, in our present temperature range, which agree with the above TG-DSC and XRD results (Figure 5a,b).

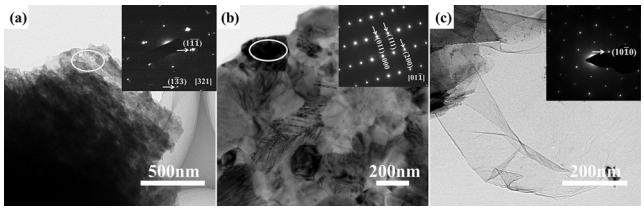

Figure 6. a),b) Typical bright-field TEM images of the vacuum annealed $Ti_3C_2T_z$ after ultrasonication; insets in (a,b) are SAED patterns corresponding to areas marked in red. c) Typical bright-field TEM image of the vacuum annealed $Zr_3C_2T_z$ after ultrasonication; inset in (c) is SAED pattern of the observed flake.

To understand the mechanism for the improved structural stability of the 2D $Zr_3C_2T_z$, the binding energy describing structure stability were studied. The bare 2D Ti_3C_2 and Zr_3C_2 MXenes, together with the bulk TiC and ZrC crystals were investigated. The binding energy is defined as follows:

$$E_{\text{binding}} = (\sum_i n_i \, E_{\text{atom}} - E_{\text{system}}) / \sum_i n_i \qquad (4)$$

where n_i is the atom number for each type atom, E_{atom} is the energy of an isolated atom, and E_{system} is the total energy of the system investigated. The binding energies of our four investigated materials are given in the Supporting Information, Table S1. Our results show that the binding energy of the bulk TiC is determined to be 8.741 eV, which is larger than that 8.080 eV of Ti_3C_2 MXene. Thus, the Ti_3C_2 MXene is inclined to transform into the more stable TiC configuration under high temperature, as the experimental results show.[15] However, 2D Zr_3C_2 presents a slightly higher binding energy than that of bulk ZrC, and thus the 2D $Zr_3C_2T_z$ MXene can easier retain its 2D nature at elevated temperatures. The above calculated binding energy explains well the difference in structure stabilities between the $Ti_3C_2T_z$ and $Zr_3C_2T_z$ MXenes. Owing to the higher stability, the 2D $Zr_3C_2T_z$ may be useful for potential applications under high-temperature conditions.

Since MXenes are normally functionalized by the oxygen, fluorine, and hydroxy groups[20,44] we further investigated the

basic structural, mechanical, and electronic properties of the monolayer $Zr_3C_2T_2$ (T = O,F,OH). Considering four different structural models followed by Xie's work,[45] the stable atomic configurations of the 2D $Zr_3C_2T_2$ were all determined. The top-view and side-view of the 2D $Zr_3C_2T_2$ are given in Figure 7a and b, respectively. The functional groups T are on

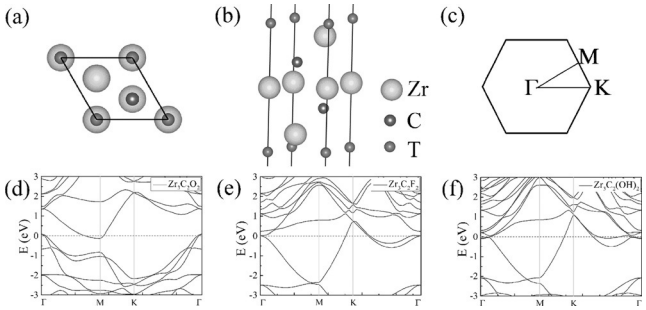

Figure 7. a) Top view and b) side view of the 2D $Zr_3C_2T_2$ (T = O, F, OH). c) The Brillouin zone of the 2D hexagonal lattice. d), e), f) The electronic energy bands of $Zr_3C_2O_2$, $Zr_3C_2F_2$, and $Zr_3C_2(OH)_2$, respectively.

the top sites of the middle zirconium atoms. The space group of the unit cell is $P\bar{3}m1$ (164), and the corresponding Brillouin zone (BZ) of the 2D hexagonal lattice is given in Figure 7c. The relaxed lattice parameters of the three 2D carbides investigated are given in the second column of Table 1.

Table 1: The structural parameters and elastic constants of the 2D $Zr_3C_2T_2$ (T = O,F, and OH).

System	*a* [Å]	*d* [Å]	c_{11} [GPa]	c_{12} [GPa]
Ti_3C_2	3.097	7.237	335.5	66.29
Zr_3C_2	3.336	7.990	295.2	60.93
$Zr_3C_2O_2$	3.314	9.475	392.9	117.7
$Zr_3C_2F_2$	3.332	10.19	293.0	75.68
$Zr_3C_2(OH)_2$	3.330	11.31	270.4	64.69

Evidently, the oxygen functionalized $Zr_3C_2O_2$ presents a smaller lattice parameter compared to those of $Zr_3C_2F_2$ and $Zr_3C_2(OH)_2$. This behavior is due to the stronger interaction between the oxygen groups and the surface zirconium atoms, and which has been well-studied for the M_2CT_2 MXenes in our previous work.[44] The mechanical strengths of the $Zr_3C_2T_2$ and the bare M_3C_2 (M = Ti, Zr) MXenes meantioned were also determined, which were calculated from Equation (5):

$$c_{ij} = c_{ij,\mathrm{cell}}(c/d) \quad (5)$$

where $c_{ij,\mathrm{cell}}$ is the elastic constants estimated from the MXene unit cell, c is the lattice parameter perpendicular to MXene surface, and it is equal to 30 Å in our simulation. d is the layer thickness, which is chosen as the distance between the top-surfaces of two neighboring monomers in the multilayer MXenes, similar to the work of Fei and Yang for phosphorene.[46] All the layer thicknesses (d), the calculated elastic constants c_{11} and c_{12} are given in Table 1. The layer thicknesses presented here are monolayer thicknesses without considering intercalated species, and are thus smaller than the experimental results. The mechanical strength c_{11} for $Zr_3C_2O_2$ is determined as high as 392.9 GPa. This manifests that the $Zr_3C_2O_2$ can be a good choice used in composite structural materials. The electronic energy bands of the 2D $Zr_3C_2T_2$ (T = O, F, OH) are provided in Figure 7e,f are the electronic energy bands of the 2D $Zr_3C_2O_2$, $Zr_3C_2F_2$, and $Zr_3C_2(OH)_2$, respectively. All of the three 2D carbides are metallic with electronic energy branches crossing their Fermi levels.

In summary, we synthesized the 2D $Zr_3C_2T_x$ MXene for the first time from parent ternary layered $Zr_3Al_3C_5$, which provides a new approach for the synthesis of Zr- and potentially Hf-containing MXenes. Based on DFT calculations, the structural, electronic and elastic properties of our obtained $Zr_3C_2T_z$ MXenes have been determined. All of the three functionalized $Zr_3C_2T_2$ (T = O, F, OH) MXenes exhibit metallic behavior, and $Zr_3C_2O_2$ presents the strongest mechanical strength with a c_{11} value of 392.9 GPa. Compared to $Ti_3C_2T_z$ MXene, $Zr_3C_2T_z$ has better structural stability in vacuum or argon atmosphere. It is reasonable to assume that the newly developed 2D $Zr_3C_2T_z$ MXenes will have promising potential applications ranging from electrode materials in electrical energy storage, reinforcement fillers for polymers, to sensors and catalysts, especially when served in a relatively high-temperature environment.

Acknowledgements

The present work was supported by the National Natural Science Foundation of China (Grant No. 91226202 and 91426304), the "Strategic Priority Research Program" of the Chinese Academy of Sciences (Grant No. XDA02040105 and XDA03010305), ITaP at Purdue University for computing resources, CAS Interdisciplinary Innovation Team Project, and the Major Project of the Ministry of Science and Technology of China (Grant No. 2015ZX06004-001). P. Eklund also aknowledges the Swedish Foundation for Strategic Research (SSF) through the Future Research Leaders 5 program and the Synergy Grant FUNCASE.

Keywords: carbides · layered structures · nanosheets · selective extraction · thermal stability

How to cite: *Angew. Chem. Int. Ed.* **2016**, *55*, 5008–5013
Angew. Chem. **2016**, *128*, 5092–5097

[1] K. S. Novoselov, A. K. Geim, S. V. Morozov, D. Jiang, Y. Zhang, S. V. Dubonos, I. V. Grigorieva, A. A. Firsov, *Science* **2004**, *306*, 666–669.
[2] H. Zhang, *ACS Nano* **2015**, *9*, 9451–9469.
[3] M. Xu, T. Liang, M. Shi, H. Chen, *Chem. Rev.* **2013**, *113*, 3766–3798.
[4] M. Naguib, Y. Gogotsi, *Acc. Chem. Res.* **2015**, *48*, 128–135.
[5] V. Singh, D. Joung, L. Zhai, S. Das, S. I. Khondaker, S. Seal, *Prog. Mater. Sci.* **2011**, *56*, 1178–1271.

[6] A. Gupta, T. Sakthivel, S. Seal, *Prog. Mater. Sci.* **2015**, *73*, 44 – 126.
[7] J. N. Coleman, M. Lotya, A. O'Neill, S. D. Bergin, P. J. King, U. Khan, K. Young, A. Gaucher, S. De, R. J. Smith, I. V. Shvets, S. K. Arora, G. Stanton, H.-Y. Kim, K. Lee, G. T. Kim, G. S. Duesberg, T. Hallam, J. J. Boland, J. J. Wang, J. F. Donegan, J. C. Grunlan, G. Moriarty, A. Shmeliov, R. J. Nicholls, J. M. Perkins, E. M. Grieveson, K. Theuwissen, D. W. McComb, P. D. Nellist, V. Nicolosi, *Science* **2011**, *331*, 568 – 571.
[8] R. C. Andrew, R. E. Mapasha, A. M. Ukpong, N. Chetty, *Phys. Rev. B* **2012**, *85*, 125428.
[9] C. Lee, X. Wei, J. W. Kysar, J. Hone, *Science* **2008**, *321*, 385 – 388.
[10] A. H. Castro Neto, F. Guinea, N. M. R. Peres, K. S. Novoselov, A. K. Geim, *Rev. Mod. Phys.* **2009**, *81*, 109 – 162.
[11] A. A. Balandin, S. Ghosh, W. Bao, I. Calizo, D. Teweldebrhan, F. Miao, C. N. Lau, *Nano Lett.* **2008**, *8*, 902 – 907.
[12] Y. Zhu, S. Murali, W. Cai, X. Li, J. W. Suk, J. R. Potts, R. S. Ruoff, *Adv. Mater.* **2010**, *22*, 3906 – 3924.
[13] S. Z. Butler, S. M. Hollen, L. Cao, Y. Cui, J. A. Gupta, H. R. Gutiérrez, T. F. Heinz, S. S. Hong, J. Huang, A. F. Ismach, E. Johnston-Halperin, M. Kuno, V. V. Plashnitsa, R. D. Robinson, R. S. Ruoff, S. Salahuddin, J. Shan, L. Shi, M. G. Spencer, M. Terrones, W. Windl, J. E. Goldberger, *ACS Nano* **2013**, *7*, 2898 – 2926.
[14] M. Naguib, V. N. Mochalin, M. W. Barsoum, Y. Gogotsi, *Adv. Mater.* **2014**, *26*, 982 – 982.
[15] M. W. Barsoum, *Prog. Solid State Chem.* **2000**, *28*, 201 – 281.
[16] P. Eklund, M. Beckers, U. Jansson, H. Högberg, L. Hultman, *Thin Solid Films* **2010**, *518*, 1851 – 1878.
[17] M. Naguib, O. Mashtalir, J. Carle, V. Presser, J. Lu, L. Hultman, Y. Gogotsi, M. W. Barsoum, *ACS Nano* **2012**, *6*, 1322 – 1331.
[18] J. Halim, M. R. Lukatskaya, K. M. Cook, J. Lu, C. R. Smith, L.-Å. Näslund, S. J. May, L. Hultman, Y. Gogotsi, P. Eklund, M. W. Barsoum, *Chem. Mater.* **2014**, *26*, 2374 – 2381.
[19] M. Naguib, M. Kurtoglu, V. Presser, J. Lu, J. Niu, M. Heon, L. Hultman, Y. Gogotsi, M. W. Barsoum, *Adv. Mater.* **2011**, *23*, 4248 – 4253.
[20] M. Khazaei, M. Arai, T. Sasaki, C.-Y. Chung, N. S. Venkataramanan, M. Estili, Y. Sakka, Y. Kawazoe, *Adv. Funct. Mater.* **2013**, *23*, 2185 – 2192.
[21] H. Fashandi, V. Ivády, P. Eklund, A. L. Spetz, M. I. Katsnelson, I. A. Abrikosov, *Phys. Rev. B* **2015**, *92*, 155142.
[22] M. R. Lukatskaya, O. Mashtalir, C. E. Ren, Y. Dall'Agnese, P. Rozier, P. L. Taberna, M. Naguib, P. Simon, M. W. Barsoum, Y. Gogotsi, *Science* **2013**, *341*, 1502 – 1505.
[23] X. Liang, A. Garsuch, L. F. Nazar, *Angew. Chem. Int. Ed.* **2015**, *54*, 3907 – 3911; *Angew. Chem.* **2015**, *127*, 3979 – 3983.
[24] M. Naguib, J. Come, B. Dyatkin, V. Presser, P.-L. Taberna, P. Simon, M. W. Barsoum, Y. Gogotsi, *Electrochem. Commun.* **2012**, *16*, 61 – 64.
[25] X. Wang, S. Kajiyama, H. Iinuma, E. Hosono, S. Oro, I. Moriguchi, M. Okubo, A. Yamada, *Nat. Commun.* **2015**, *6*, 6544.
[26] M. Naguib, J. Halim, J. Lu, K. M. Cook, L. Hultman, Y. Gogotsi, M. W. Barsoum, *J. Am. Chem. Soc.* **2013**, *135*, 15966 – 15969.
[27] M. Ghidiu, M. R. Lukatskaya, M.-Q. Zhao, Y. Gogotsi, M. W. Barsoum, *Nature* **2014**, *516*, 78 – 81.
[28] B. Anasori, Y. Xie, M. Beidaghi, J. Lu, B. C. Hosler, L. Hultman, P. R. C. Kent, Y. Gogotsi, M. W. Barsoum, *ACS Nano* **2015**, *9*, 9507 – 9516.
[29] R. Meshkian, L.-Å. Näslund, J. Halim, J. Lu, M. W. Barsoum, J. Rosen, *Scr. Mater.* **2015**, *108*, 147 – 150.
[30] C. Hu, C. C. Lai, Q. Tao, J. Lu, J. Halim, L. Sun, J. Zhang, J. Yang, B. Anasori, J. Wang, Y. Sakka, L. Hultman, P. Eklund, J. Rosen, M. W. Barsoum, *Chem. Commun.* **2015**, *51*, 6560 – 6563.
[31] C. C. Lai, R. Meshkian, M. Dahlqvist, J. Lu, L. Å. Näslund, O. Rivin, E. N. Caspi, O. Ozeri, L. Hultman, P. Eklund, M. W. Barsoum, J. Rosen, *Acta Mater.* **2015**, *63*, 157 – 164.
[32] C. Xu, L. Wang, Z. Liu, L. Chen, J. Guo, N. Kang, X.-L. Ma, H.-M. Cheng, W. Ren, *Nat. Mater.* **2015**, *14*, 1135 – 1141.
[33] Y.-C. Zhou, L.-F. He, Z.-J. Lin, J.-Y. Wang, *J. Eur. Ceram. Soc.* **2013**, *33*, 2831 – 2865.
[34] J. Zhou, F. Qiu, L. Shen, F. Li, J. Xue, M. W. Barsoum, Q. Huang, *J. Am. Ceram. Soc.* **2014**, *97*, 1296 – 1302.
[35] O. Mashtalir, M. Naguib, V. N. Mochalin, Y. Dall'Agnese, M. Heon, M. W. Barsoum, Y. Gogotsi, *Nat. Commun.* **2013**, *4*, 1716.
[36] Q. Tang, Z. Zhou, *Prog. Mater. Sci.* **2013**, *58*, 1244 – 1315.
[37] C. Morant, J. M. Sanz, L. Galán, L. Soriano, F. Rueda, *Surf. Sci.* **1989**, *218*, 331 – 345.
[38] A. P. Rizzato, C. V. Santilli, S. H. Pulcinelli, Y. Messaddeq, P. Hammer, *J. Sol-Gel Sci. Technol.* **2004**, *32*, 155 – 160.
[39] M.-P. Crosnier-Lopez, F. Le Berre, J.-L. Fourquet, *J. Mater. Chem.* **2001**, *11*, 1146 – 1151.
[40] J. Li, Y. Du, C. Huo, S. Wang, C. Cui, *Ceram. Int.* **2015**, *41*, 2631 – 2635.
[41] Z. Li, L. Wang, D. Sun, Y. Zhang, B. Liu, Q. Hu, A. Zhou, *Mater. Sci. Eng. B* **2015**, *191*, 33 – 40.
[42] T. El-Raghy, M. W. Barsoum, M. Sika, *Mater. Sci. Eng. A* **2001**, *298*, 174 – 178.
[43] M. W. Barsoum, T. El-Raghy, L. Farber, M. Amer, R. Christini, A. Adams, *J. Electrochem. Soc.* **1999**, *146*, 3919 – 3923.
[44] X. H. Zha, K. Luo, Q. Li, Q. Huang, J. He, X. Wen, S. Du, *Europhys. Lett.* **2015**, *111*, 26007.
[45] Y. Xie, P. R. C. Kent, *Phys. Rev. B* **2013**, *87*, 235441.
[46] R. Fei, L. Yang, *Nano Lett.* **2014**, *14*, 2884.

Received: November 16, 2015
Revised: January 6, 2016
Published online: March 9, 2016

